OPEN

The role of filopodia in the recognition of nanotopographies

Jörg Albuschies & Viola Vogel

Department of Health Sciences and Technology, ETH Zurich, CH-8093 Zurich, Switzerland.

Substrate-exploring functions of filopodia were previously suggested based on cell studies on flat surfaces, but their role in topography sensing especially within nanofibrillar environments remained elusive. Here we have grown highly flexible hairy silicon nanowires on micropatterned islands on otherwise flat glass surfaces and coated them both with the extracellular matrix (ECM) protein fibronectin. This allowed us to visualize how filopodia steer fundamental cell functions such as cell adhesion, spreading, migration and division in the absence of lamellipodia. Shortly after seeding, transient filopodia protrude from the still spherical cells. Once filopodia contact nanowires, they bend and align them, while most filopodia peel off from flat surfaces. A zipping mechanism regulated by traction forces is proposed to explain how force-induced changes in filopodia-substrate contact angles enable topography sensing, including the still elusive phenomenon of contact guidance. Filopodia thus play a central role in steering transient topographic preferences.

Cellular processes have traditionally been studied for cells adhering to flat surfaces with a focus on lamellipodia. While filopodia were first described in living cells in 1961[1], their substrate-exploring functions were suggested in 1976 and assumed to be regulated by mechanical forces[2]. Lamellipodia and filopodia are both actin based cell protrusions but having a distinct actin architecture and internal geometrical organization. Lamellipodia are based upon a thin sheet-like branched network of actin filaments, whereas filopodia are highly organized and tightly cross-linked long bundles of unidirectional and parallel actin filaments[3]. Various filopodial functions are now well established, ranging from directing the growth cones in neural networks[4–6] while axons become disoriented when filopodia formation was suppressed[7,8], to epithelial sheet closure via cell-cell-zipping[9], as well as platelet aggregation and blood clotting[10]. Also their sensing roles on rough surfaces were described[11–13], as well as their entanglement in 3D collagen matrices[14,15]. Yet, no conclusive mechanism has been proposed how filopodia can recognize topographical features and which role filopodia traction forces play in directing cell orientation and migration.

Various cell types express high levels of more than 10 μm long transient filopodia in their spherical state prior spreading[16,17], either after trypsinization from cell culture dishes[16,18] or during mitosis[17,19]. The occurrence of transient filopodia pointing in all directions, while the cell shape is still spherical and largely detached from the surrounding matrix, suggests a highly conserved role of filopodia in mediating initial adhesion events and in exploring environmental features. On flat surfaces these transient filopodia are known to quickly disappear during spreading in favor of the widely described lamellipodia mediated spreading mechanism[16,20,21], which is why the recent literature mainly described cell spreading of newly seeded cells on flat surfaces with a focus on lamellipodia[21–24]. The role of filopodia for cell spreading dynamics was explicitly described as of minor importance in the context of flat environments[25]. An extended time period passes between cell seeding and spreading, commonly defined as lag time[20,23,26]. It was reported that the rigidity of polyacrylamide gels[27], density of ECM molecules[20,28] and the silencing (knock out or knock downs) of some proteins involved in the cell adhesome[29] can affect the length of the lag period and also the cell spreading rate[20,28]. Despite this rich literature on molecular mechanisms that regulate the formation, composition and adhesion of filopodia to 2D surfaces (for reviews see[30–32]), little attention was given to the question whether and how traction forces transmitted by filopodia to ECM anchorage sites regulate any of the above described phenomena. Surprisingly, it was also not asked whether filopodia could play a role in mediating the first contacts during the lag time.

Novel nanoengineered substrates allowed us for the first time to capture how filopodia interact with nanofibrillar structures, and subsequently bend and align them by traction forces. Shortly after cell adhesion, we describe how cells transition from a filopodia-rich spherical cell state to a lamellipodia-dominated state that enables cell spreading on flat surfaces. In contrast, filopodia enable cell orientation and spreading within 3D nanofibrillar environments and these processes are steered by filopodia traction forces reaching into the nN range.

Results

Fabrication of arrays of nanowire bushels on otherwise flat glass surfaces. To better understand the role of initial filopodia in sensing nanofibrillar environments, we introduce here a novel micropatterned silicon nanowire substrate that mimics essential fibrillar aspects of native tissue on the nanoscale. These hairy silicon nanowires (NWs) with 40 nm in diameter and 5–10 µm in length were grown on 5 and 10 µm wide islands with 20 and 40 µm separation on microscopy glass slides, utilizing a vapor-liquid-solid (VLS) process[33] (Fig. 1a–e). In contrast to stiff vertical nanoneedles[34–36], these thin silicone nanowires are highly flexible[37,38] and can thus be spatially re-oriented by the forces applied by individual filopodia. Their diameters are in the range of fibronectin and collagen ECM fibrils[39,40]. Confocal microscopy and electron microscopy allowed us to capture how initial transient filopodia contact and subsequently align with nanofibrils and how this affected the most elementary cellular processes of adhesion, spreading, migration and division. The NW growth from 40 nm gold colloids on amorphous glass substrates yields surface anchored and randomly oriented single crystalline NWs (Fig. 1f–h). The surface of silicon NWs presents a native oxide layer, which allows identical chemical functionalization of NWs and the underlying glass surface with fibronectin[41]. Patterned islands of nanowires surrounded by flat surfaces enabled us to study the competition of different topographical cues on cell behavior.

Prior to cell spreading, the spontaneous formation of transient filopodia is significantly upregulated. For cells in suspension and prior spreading, the formation of transient filopodia is significantly upregulated. In agreement with the literature[2,16], we show here that
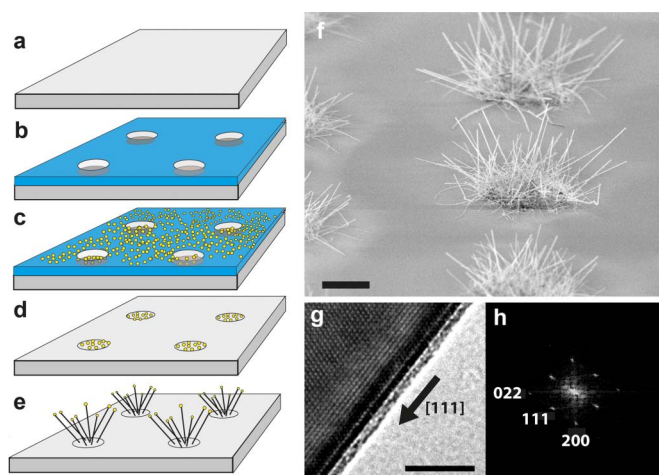

Figure 1 | Fabrication and characterization of silicon nanowires (NWs) on glass. (a) Microscope cover slips (b) were patterned with optical lithography to (c) locally deposit 40 nm Au colloids in micropatterned arrays. (d) Au colloids on separated islands served as (e) nucleation catalysts to grow randomly oriented silicon nanowires. (f) The SEM micrograph shows in bird's eye view the micropatterned islands of Vapor-Liquid-Solid (VLS) grown silicon nanowires with length of 5-10 µm and 40 nm in diameter. (g) Single crystallinity of NWs was confirmed by high-resolution transmission electron microscopy (TEM). The crystal orientation is <111> along the SiNW growth axis as indicated by the black arrow. Silicon has an anisotropic modulus of elasticity depending on the crystal orientation. The elastic modulus of Si along the <111> orientation is 169 GPa, which is used for calculation of NW spring constants. A 1–2 nm thin native amorphous SiO_2/SiO_x layer is clearly visible on the NW surface in the TEM micrograph. (h) The crystal orientation was determined from TEM images with "CRSIP" software for advanced crystallographic analysis. Scale bars f = 5 µm, g = 5 nm.

spherical fibroblasts freshly seeded to a substrate after trypsinization expressed >10 µm long filopodia (Fig. 2a, e, h), and we counted up to 200 filopodia per cell. Upon first contact with the substrate, the spheroid bulk part of these fibroblasts is separated from the surface by large amounts of filopodia connecting the cell body to the substrate (Fig. 2e). Filopodia thus initiated the first substrate contacts at a time where no ruffles and no lamellipodia were present (Fig. 2a, e, h).

On 2D surfaces, transient filopodia mostly peeled off while the remaining filopodia eventually nucleated lamellpodia. Quantitative analysis of 20 cells showed that initial filopodia mostly peeled off from flat substrates decreasing from approx. 200 to 40 ± 14 within 5 min (Fig. 2b) thereby delaying cell spreading, while the remaining surface anchored filopodia got straightened-out over time (Fig. 2b). The SEM images in Fig. 2b (Supp. Fig. S1c) revealed that all remaining adherent filopodia had formed rather shallow angles with distal surface contacts. It was reported previously that transient filopodia form during the lag time and define initial adhesion events, which are followed subsequently by lamellipodia-mediated cell spreading[2,16]. It was also previously reported that individual filopodia with distal surface contacts to micropatterned adhesive areas can nucleate lamellipodia via rac1 signaling at their tips[42]. At later time points (~10 min) we could observe the formation of lamellipodia from filopodia tips (Suppl. Fig. S1b).

Cell spreading on flat surfaces later proceeded in the previously described sequence[2,16,20,23,26]: after passing an initial lag period, cell spreading is initiated by sporadic filopodia-substrate contacts, which finally resulted in a replacement of transient filopodia by a circumferential lamellipodium (Fig. 2a–d). After 30 minutes, only 31 ± 12 filopodia with length of 1–3 µm were located at the leading edge of the lamellipodium (Fig. 2c, d). Not reported previously, a major decrease of the number of transient filopodia was seen during the lag period (<5 min) while cells were still spherical (Fig. 2a, b).

Initial filopodia aligned quickly with individual nanowires and formed long lasting adhesions. On densely NW decorated surfaces, transient filopodia aligned already within the first few minutes with individual NWs and formed long lasting adhesions without the formation of a lamellipodium (Figure 2h–l). Within the first 5 minutes, these initial filopodia aligned tightly with individual nanowires over distances of several micrometer (Fig. 2i'' arrowheads and Fig. 2i'''). Aligned filopodia-nanowire adhesions were oriented towards the cell body and showed steeper angles compared to filopodia adhesions formed on flat surfaces. Micron-wide conical membrane protrusions appeared within the first 5 minutes after cell seeding and were guided along the straightened filopodia-NW contacts towards the adhesion sites (Fig. 2i, Suppl. Fig. S1d). After 30 min, the cells acquired dendritic cell shapes with long conical protrusions and numerous actin-rich filopodia around the cell periphery anchored to the substrate (Fig. 2l). The black planes in the confocal 3D reconstruction in Figure 2l help to visualize how the actin cytoskeleton of filopodia penetrates the dense 3D-NW substrates in z-direction. These dendritic cell shapes persisted for at least 16 hours for those cells that contacted only nanowires (Fig. 2k, l). Similar dendritic cell shapes were previously observed for fibroblasts in cell derived 3D extracellular matrix[43–45], 3D collagen gels[14] and electrospun 3D scaffolds[46,47], however the filopodia rich-morphology was not described before.

At flat versus nanofibrillar interfaces, filopodia preferentially adhered to NWs and completely retracted from flat surfaces. While freshly seeded cells made their very first filopodia contacts to both topographies (Fig. 2e, e'), the initial filopodia quickly adhered to and then aligned with nanowires by pulling on them (Fig. 2f, g). In contrast, the majority of filopodia touching the flat
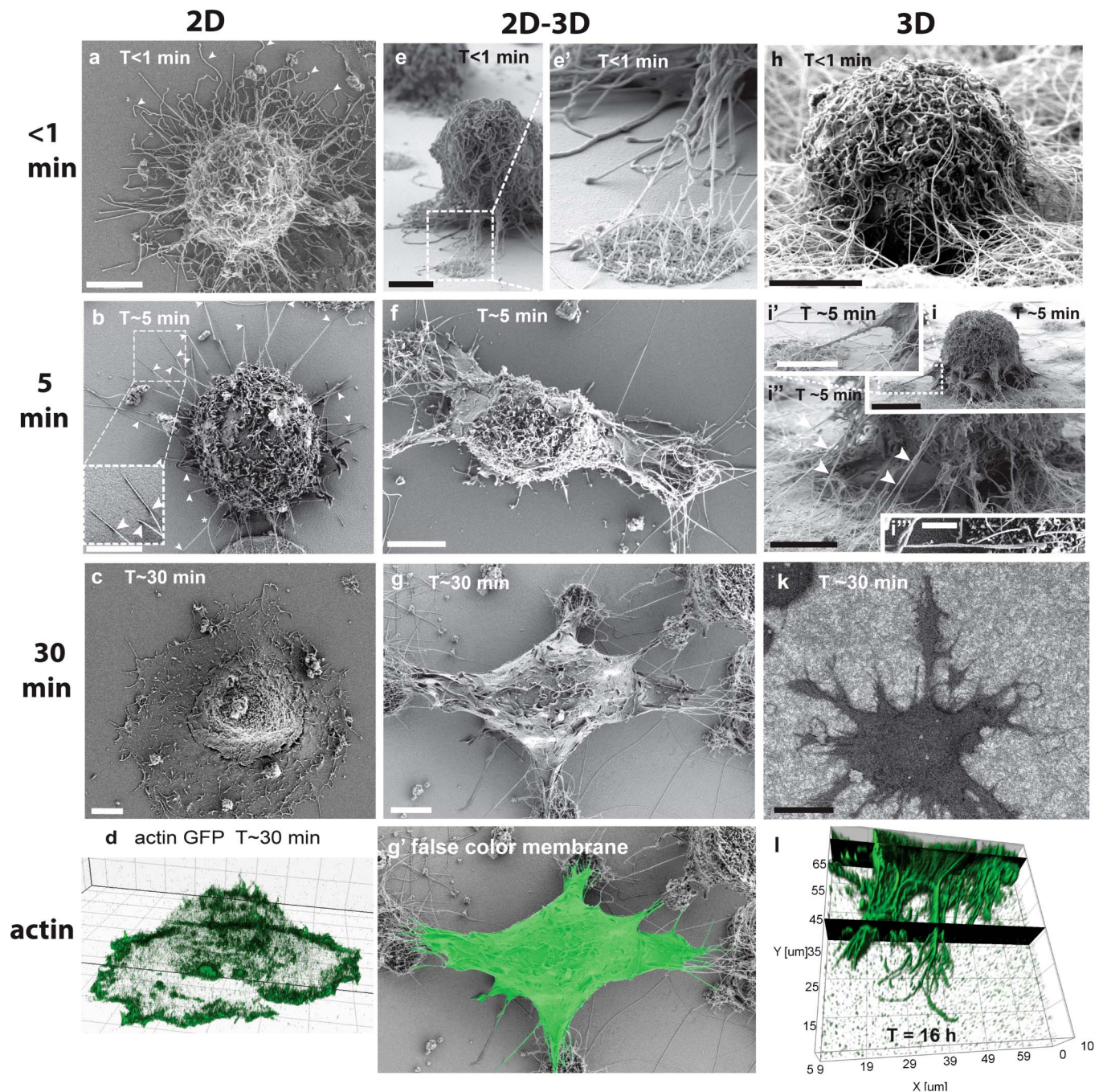
Figure 2 | Time-dependent spreading events of fibroblasts on flat surfaces and in contact with NWs. (a–d) Fibroblasts spreading on fibronectin (Fn) coated flat glass surfaces (2D). Large numbers of >10 µm long filopodia cover the entire surface of spherical cells in the first moment of substrate contact. (a arrowheads) Straight and curled filopodia are deposited randomly around the cell periphery. (b arrowheads) Within the first 5 min, most filopodia retracted and only few straight filopodia remained with distal substrate adhesions touching the surfaces under a shallow angle (kink). (c) Cells spread with a circumferential lamellipodium after passing the lag time. (d) The actin-rich lamellipodium replaced the initial surface adherent filopodia contacts (live cell imaging with actin GFP transfected cells). (e) On flat versus fibrillar interfaces, transient filopodia were initially in contact with both, flat surfaces and nanowires. (f) The transient filopodia adhered and aligned with individual nanowires and quickly directed cell spreading towards nanowire adhesion sites, while most filopodia retracted from the Fn coated flat glass surfaces. (g and Suppl. Fig. S1e) The apical membrane that is not facing nanowires was later completely depleted of filopodia, while ruffles appeared after 30 min. (g′) The false color membrane image illustrates that no lamellipodia were formed at the flat surfaces in between nanowire islands, in contrast (c, d) to flat substrates, where a full circumferential lamellipodum had occurred after the same time period. (h, i) Initial filopodia formed entangled and centripetally aligned adhesions to individual nanowires when in contact with densely NW decorated substrates. (I and Suppl. Fig. S1d) Aligned filopodia-NW adhesions guided pseudopods/membrane protrusions towards the NW anchorage site. (k) Filopodia-mediated cell spreading lead to dendritic cell shapes in the absence of typical lamellipodia-like membrane protrusions. (l) Confocal 3D reconstruction of phalloidin-alexa 546 stained actin cytoskeleton after 16 hours on 3D nanowires shows dendritic cell protrusions that display numerous filopodia, which are anchored deeply into the nanowire matrix in the absence of lamellipodia. Scale bars 5 µm with the exception of i, k = 10 µm and i ′″ = 1 µm.

surface peeled off (Fig. 2f). Despite the adhesive fibronectin coating on the flat surface, the filopodia disappeared completely within the first 5 minutes leaving only a filopodia-depleted membrane behind (Fig. 2f, g). The cells that were located in between 20 μm separated nanowire islands showed cell protrusions towards both NW islands in opposing directions (Fig. 2f). The membrane protrusions in contact with the nanowires contained many bundled filopodia while membrane veils advanced in between the filopodia towards these distal adhesion sites (Fig. 2f, g). After 30 min, the cells typically acquired elongated shapes often even bridging two separate nanowire islands (Fig. 2g). At this stage, even the apical membranes were completely depleted of transient filopodia (Fig. 2g). After approximately 30 min, small membrane ruffles appeared on the filopodia-depleted apical membranes (Fig. 2g, Suppl. Fig. S1e). With considerable time delay (>30 min), those membrane ruffles stabilized as they turned into precursors of lamellipodia (in agreement with previous observations[18]) that finally formed on the flat surface and thus also between nanowire islands. Once a lamellipodium had formed in contact with a flat surface, the filopodia-NW contacts were ultimately retracted (data not shown).

Dynamics of filopodia-substrate interactions. To gain insights into the mechanisms that stabilize early filopodia adhesions on flat surfaces versus flexible NWs, optical confocal time-lapse microscopy was performed, and the deflection of individual NWs via filopodia traction forces was quantified by SEM. Initial filopodia that adhered to flat substrates typically originated from random locations on the cell body, and thus at certain distances above the surface. These filopodia thus contacted the underlying substrate under a broad range of angles (Fig. 2e). Time-lapse movies showed that a kink is often seen in the filopodium, i.e. a contact point where the filopodium is kinking away from the substrate towards the elevated cell body. The sequence of optical images in Figure 3 show how a kink was advancing towards the filopodial tip and thus away from the cell body. The filopodium peeled off the flat surface with a velocity of 1 μm/min, while the filopodium at the tip shows continuous outgrowth (Figure 3a). The kink advancement slowed down and finally stopped between 5 and 7.5 min (Fig. 3a). Equally important, at the same time when the kink movement stopped, a membrane protrusion originated at the root of the filopodium and moved towards the stabilized filopodium-substrate contact (Fig. 3a arrows). A second optical microscopy (DIC) time-lapse series (Fig. 3b) captured how a fibroblast approached a nanowire island. It took 3 min until the spherical fibroblast overcame the 8 μm separation between the cell body and a NW island by forming a directed membrane protrusion/pseudopod towards the NWs. Since the contacted NWs aligned with the filopodia, the cells were subsequently guided towards the NW anchorage points (Fig. 2f and 2g).

These silicon NWs can further be utilized as force sensors due to their low bending spring constant, which is around 1 pN/nm[38]. A series of time-lapse optical microscopy images captures the kinetics by which a ~4.1 μm long nanowire was deflected as far as 2.3 μm from its initial position (Fig. 3c). To gain an estimate of the forces that filopodia can apply to individual NWs, a single filopodium-NW contact was imaged by SEM, whereby a force-bearing filopodium (Fig. 3d arrowhead) was actively broken by the electron-beam allowing the force-free NW to snap back into its resting position (Fig. 3d–f). Cells were fixed 5 min after cell seeding, and imaged in SEM without metal sputter coating. The focused electron-beam of the SEM was utilized to cut the force-bearing filopodium at both sides of the filopodium-NW contact (Fig. 3e inset). Since their deflection is described by Hooke's law[48,49], we can estimate a filopodium traction force of approximately 1.9 nN. A similar range of filopodia traction forces was previously reported when probing the deflection of obstacle neurites by neuronal growth cone filopodia (0.5–0.9 nN)[50], and
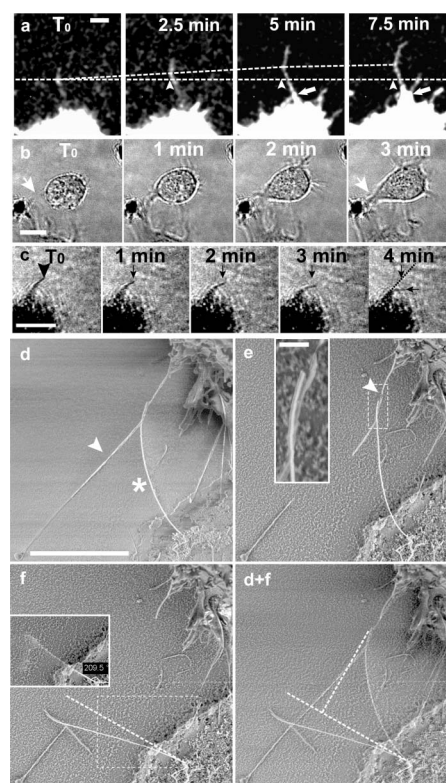

Figure 3 | Dynamics by which a filopodium is peeled off from a flat surface and probing the force applied to a single NW. (a) Time-lapse confocal series showing how a kink formed between filopodium and flat substrate advanced towards the filopodial tip (bottom slice of a confocal stack). The lower dashed line and arrowheads indicate the initial position of the kink while the upper dashed line shows the kink advancement as cell traction forces peel the filopodium off from the glass surface. The total kink advancement in this time window is 4 μm. After the peeling process slows down/terminates (> 5 min), a conical membrane protrusion emerged and moved from the cell body along the filopodium shaft (arrows). The filopodium continued to grow by additional 8 μm at the tip during the proximal peeling process. (b) A 3 min DIC time-lapse series showing how a spherical cell that just 'landed' nearby a NW island after seeding, advanced towards the NWs and closed an 8 μm wide gap in between the spherical cell cortex and the NW island by forming a several microns wide conical membrane protrusion (white arrows, also compare to Fig. 2e, f). (c) Four minutes of optical transmission microscopy show how a ~4.1 μm long nanowire was deflected ~2.1 μm from its original position within 4 min. The black arrows denote the initial and final position of the nanowire tip after 4 min. Filopodia could not be resolved with this microscopy technique. (d–e) The SEM micrograph shows a fibroblast that was fixed 5 min after seeding (compare Fig. 2b asterisk). (d, e arrowheads) A force bearing and NW-deflecting filopodium was cut off via a focused electron beam on both sides of the contact. (e-inset) The inset is a magnification of the aligned filopodium-NW contact. (f-inset) The NW restored its original position after cutting off the force-applying filopodium. Immediately after cutting, the freely suspended NW oscillated around its original force-free position and could thus not be imaged properly in this state. The anchorage point of the NW could be visualized and allowed the determination of the original NW resting position as shown by the dashed line in Fig. 3f. (f) The NW accumulated charges on the insulating substrate during imaging and finally immobilized on the substrate due to electrostatic forces (No metal coating). (d+f) The overlay of both images, before and after cutting the filopodium, allowed to quantify the deflection of the NW from its original position to be 3 μm. With a length of 4.35 μm, 38 nm in diameter and an elastic modulus of 169 GPa, the spring constant of this nanowire was 0.63 pN/nm. This resulted in 1.9 nN filopodia traction force. Scale bars b = 10 μm; a, c = 5 μm; d, e, f = 3 μm, e-inset = 200 nm.

also for filopodia adhering in parallel to compliant 2D gels (1.2 nN)[51]. Importantly, all of the fragile filopodia in the cell vicinity were intact and not broken by the SEM preparation method, even those with very small filopodia-surface contact areas. This suggests that cell shrinkage is negligible. For the unlikely shrinking of the cell body by 20% though, the force would be 1.6 nN.

Consequently, fibroblasts can apply nN force to NWs (Fig. 3d–f). Adhesions at such displaceable filopodia-NW contacts can withstand these high forces only because the filopodia align freely swiveling nanowires in parallel to the direction of the force vector and thereby increasing the number of adhesive fibronectin-integrin bonds.

Topography preference is shifted during the cell division cycle.
Dividing cells reduce their surface anchorage in order to round up during mitosis[52,53]. They thereby retract lamellipodia while only a few retraction fibers remain in the locations where the cells were previously attached[51,52]. Although it is known that mitotic cells express elevated levels of filopodia[16,18], their role during mitosis and post-mitotic spreading was not studied previously (to the best of our knowledge).

A time-lapse series of a captured event shows how a mitotic cell that was adhering to a flat surface retracted its lamellipodium, rounded up, expressed filopodia and migrated to nearby 3D nanofibers (Fig. 4 and Supplemental Movie M4). Even before the cell divided, the cell centered itself perfectly over a 5 µm wide nanofiber island. The active translocation included the complete centering of the nucleus that was previously located next to the nanowire bundle. The cell sitting centered over the nanowire island finally divided after 45 min. One daughter cell was then pushed outwards from the nanowire island whereas the other cell stayed behind at the previous location. The daughter cell moved from its original location (black arrowhead at 45 min) towards a free surface spot where the previous mother cell was not adhering and thus having the lowest density of retraction fibers (white asterisk). The steering role of filopodia seen here for a rounded cells that had just divided is rather similar compared to that of filopodia of freshly trypsinized cells. This might suggest a similar filopodia-based selective topographic preference that might influence cell anchorage during mitosis and post-mitotic spreading.

Discussion

The introduction of highly flexible thin silicon NW of physiological dimensions allowed us for the first time to capture how the interplay of filopodia with lamellipodia orchestrates time-dependent recognition and preferences for topographical features as summarized in Figure 5. Prior to cell spreading, the spontaneous formation of transient filopodia is significantly upregulated. Filopodia initiate the very first substrate contacts to both, NWs and flat surfaces at a time where no ruffles and no lamellipodia were present (Figure 2a, 2e, 2h and

Figure 5a). As time progresses, most of the initial filopodia peeled off from flat surfaces, while the filopodia were able to pull the NWs into alignment thereby increasing the NW-filopodia contact areas as illustrated in Figures 5b–c. The time sequence of critical events as observed for fibroblasts adhering and spreading on flat surfaces (Fig. 2a–d), at interfaces between a flat surface and NW bushels (Fig. 2e–g) and when sitting on top of a NW lawn (Fig. 2h–l) is sketched in Figure 5d. Our data allowed us now to visualize how filopodia steer fundamental cell functions such as cell adhesion, spreading, migration and division.

The dynamics of the contact angle formed towards flexible objects determines whether filopodial adhesions break or mature. While filopodia pull on NWs and bend them, they align the NW in parallel to the filopodial shaft. This force-induced alignment increases the number of adhesive fibronectin-integrin bonds and thus the strength of a filopodium-NW interaction (Fig. 5a–c). Single filopodia can finally apply up to nanoNewton forces to NWs without breaking the contacts since this requires breaking many bonds in parallel (fracture in a shear geometry) (Fig. 3d–f and Fig. 5e). For any fibrillar object that can be deflected, the variable contact angle is reduced as the fiber is pulled into alignment. As the contact angle decreases, the force component acting normal to the fiber surface and thereby pulling upwards on the integrins located at the kink is reduced and this allows the filopodial adhesion to mature.

In contrast, a filopodium cannot bend the flat glass surface and the adhesive bonds at the location of the kink are mechanically strained as the cell applies tensile forces. On surfaces that cannot be sufficiently deflected, the integrin-fibronectin bonds located at the kink are broken if the normal force component is larger than the rupture force of integrins. As captured in Figure 3, the kink moves outwards towards to the tip of the filopodium thereby opening the adhesive contacts in a zipping mode, integrin-by-integrin. An outwards movement of the kink position, however, reduces the contact angle and thus the normal force acting on each integrin. Once the normal force is less than the binding strength of an integrin-fibronectin contact, the kink advancement will stop as seen in the image sequence (Fig. 3a and Suppl. Fig. S1c). During the lag period and before cells started to spread on flat surfaces, it is important to realize that transient filopodia protrude and contact flat surfaces under a wide range of angles (Fig. 2a, e). While most transient filopodia were observed to peel off on flat glass surfaces, only a small fraction of filopodia were attached under an angle that was shallow enough to stabilize filopodia-substrate contacts (Fig. 2b and Suppl. Fig. S1c).

To derive a quantitative model how cells take advantage of the dynamic contact angle, it is important to recognize that the mechanical stability of the filopodial contact enables cells to distinguish between nanofibrillar and flat substrates. Filopodia adhesions formed with rigid objects are frequently zipped open, while realignment with a flexible object transitions the contact into a far stronger
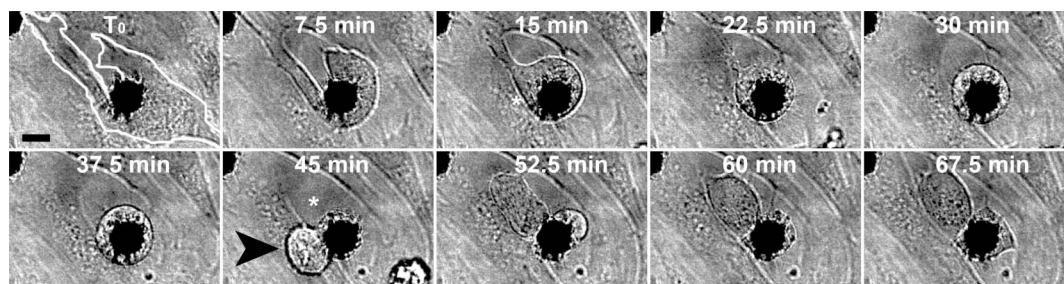

Figure 4 | A dividing fibroblast at a 2D-3D matrix interface captured in a DIC time-lapse series. The 2D-adherent fibroblast as outlined with the white line at T_0 retracted adhesions from the flat surface while rounding up for division. While the cell retracted completely from the flat surface it translocated perfectly centered over a NW island where it divided. A daughter cell, which was pushed out from the NW island (black arrowhead at 45 min) translocated to a free surface spot (white asterisk) where the mother cell previously had the smallest adhesive area (Suppl. Movie M4). Scale bar 5 µm.
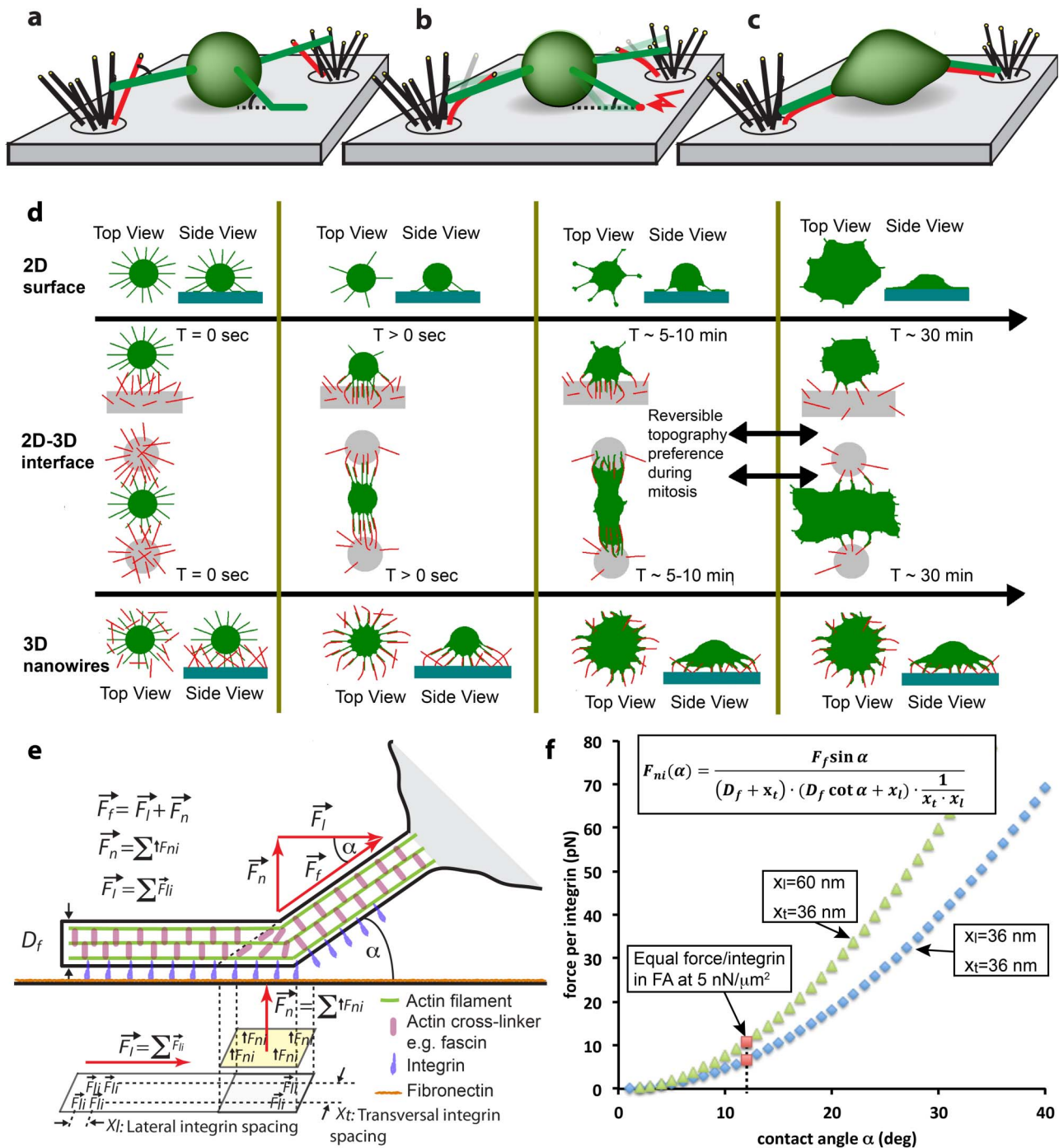
Figure 5 | Underpinning mechanisms of topography sensing. (a–c) Schematics of the topography recognizing function of filopodia. (d) Summary of our findings for the different engineered substrates and how differences in cell shape and polarity as well as the spreading dynamics are controlled by filopodia-NW interactions. (d) The first row describes for flat glass (2D) how fibroblasts undergo a rapid phase transition from filopodia-rich initial state towards a lamellipodia-mediated spreading (compare Suppl. Fig. S1b). The second row shows how cells sitting at interfaces between flat surface and NWs contact the NWs, quickly adhere, align and spread towards nanowire adhesions, while filopodia peel-off from the adjacent flat surfaces. After ~30 min, delayed lamellae/ruffle formation (Suppl. Fig. S1e) leads to migration towards the flat surface (Data not shown). This dynamic change in topography preference is reversible during mitotic rounding of fibroblasts (see Fig. 4 and Supplemental Movie M4). The bottom row shows how fibroblasts on purely nanowire decorated surfaces quickly spread via aligned filopodia-nanowire adhesions into dendritic shapes, without formation of lamellipodia. (e) Schematics showing force distributions on integrins in dependency of the angle α at which a filopodium contacts an object. (f) A simple mechanical zipping model allows to estimate the normal forces acting on individual integrins as function of the contact angle α. Since the number of integrins/μm² within the adhesions is unknown, we calculated the normal force per integrin as function of the contact angle for two integrin densities (blue and green symbols) by assuming a filopodia traction force of 2 nN. To estimate the critical angle below which peeling will stall, we next assumed that the integrins within the filopodial shaft can sustain the same force as in focal adhesions (FAs). Cells typically apply traction forces around 5 nN/μm² at focal adhesions (FA)[63]. This converts to the force per integrin as marked with red squares and thereby predicts a critical angle of close to 12° below which filopodial adhesions mature rather than peeling off before their tips detach. Supplemental figure S1c displays that only a small fraction of transient filopodia (very long ones with their base close to the flat substrate) formed angles <12°.

shear geometry with a large number of parallel bonds that have to be broken in a single event (Figure 5a–c). This same molecular zipper concept has already been demonstrated to regulate the mechanical strength of DNA–DNA contacts if the contacts are broken in a weak zipping versus strong shear-geometry[54,55]. Based on these observations and literature data, we derived an analytical mechanical model that estimates the critical contact angle above which a filopodium-substrate contact is zipped open (Figure 5e, f and see suppl. information for a detailed derivation). The forces acting on integrins that are calculated with this model as a function of the filopodia-substrate contact angle are in good agreement with the measured rupture forces from AFM experiments. A single integrin-fibronectin contact breaks at a normal force of 70 ± 5 pN at a loading rate of 1 nN/s in AFM experiments[56,57] Since the rupture force depends on the loading rate, the rupture force decays by 25–30 pN/Decade[pN/s][56,57]. A rough estimate therefore suggests that the corresponding rupture force at a loading rate of 10 pN/s is expected from AFM experiments to be around 5–25 pN. The force loading, from contacting a NW to deflecting it towards a resisting force of roughly 2 nN occurs within a few minutes which corresponds to a loading rate in the range of 10 pN/s (Fig. 3d–f).

A single mechanical concept can thus explain the events described here prior the formation of a lamellipodium (as summarized in Figure 5d): the contact angle that is formed between a spontaneously protruding filopodium and the substrate controls whether a filopodial contact matures or fractures. The angle-dependent vertical versus horizontal force components define how much total force is applied to a limited, and also angle-dependent number of integrins. The contact angle finally defines whether the contact can be mechanically stabilized or is peeled off. The force-strengthened filopodia adhesions caused by alignment with the flexible NWs thus enable a quick cell spreading (<5 min) (Fig. 2e, f). The formation of lamellipodia is delayed for 2D-3D interfaces (<30 min) (Fig. 2g) or even completely inhibited by the presence of dense 3D nanowire surfaces (Fig. 2k, l). This dynamic contact-angle model allows us to make a few general predictions regarding topography sensing and contact guidance:

First, it was recognized previously that endothelial cells apply high forces in the early minutes of spreading even in the absence of stress fibers[26]. Yet the authors were surprised by unexpectedly high forces only stating that their results are the first to show the presence of traction forces without the presence of focal adhesions. Our data now show that transient filopodia whose existence might have been missed in those recordings at lower optical resolution can exert nanoNewton traction forces even in the absence of lamellipodia and stress fibers.

Second, controversy exists regarding the questions whether cells prefer nanotopographical features or flat surfaces. Here we could show that topographical preference is not just an intrinsic and cell specific attribute. Instead, topographical preferences can change with time (Fig. 5d). In particular, switching the topographical preference can be observed during mitosis (Fig. 4). When a cell enters mitosis, the occurrence of retraction fibers was reported and it was asked whether they could play a role in post-mitotic spreading as well[52,53]. The time-lapse series (Fig. 4 and Supplemental Movie M4) showed how a previously 2D adherent cell changed its topographic preference from a 2D adherent state towards a preferential adhesion and translocation towards a NW covered area. The cell division happened centered over the nanowire islands while the contact to the surrounding flat surface was minimized. A potential role of filopodia in ECM anchorage during mitotic rounding, accelerating post-mitotic spreading and finally in guiding the direction along which the two daughter cells moved apart was not previously considered. Based on the assumption that filopodia of mitotic cells have similar properties as shown for filopodia of trypsinized cells, we suggest that the strongest forces can be exerted via filopodia (2 nN) along nanofibers immediately after cell division and might thus contribute strongly to

mitotic and post-mitotic ECM anchorage that guide subsequent spreading direction and migration. In contrast, the previously described forces during mitosis were measured at retraction fibers in the range of 200–300 pN[52].

Third, while the mechanism underpinning the phenomenon of contact guidance by topographical features remained elusive, our simple physical zipping model derived for nanofibrils can perhaps explain how other topographical features might guide cell alignment and direct cell migration as well (Figure 5). First, while the initial filopodia of a freshly seeded cell protrude in random directions (Fig. 2a), only those get stabilized that can form an adhesive contact that is sufficiently firm to withstand the cell-generated tensile forces (Fig 2f, g). Second, the direction of the force vector acting on the topographical features will determine which subset of transient filopodia has a chance to survive while the others are peeled off. Third, filopodia that are oriented more perpendicular to the topographical nanofeatures will always exhibit reduced adhesive strength as the growth of the adhesive contact gets abruptly abrogated when the filopodial kink reaches a topographic edge. This is in agreement with previously described vinculin and actin localization at the edges of grooves on nanogrooved substrates[58]. They thus have a higher likelihood to detach via the above described peeling mechanism.

Forth, the retraction dynamics of filopodia on nanogrooved substrates were analyzed earlier by time-lapse microscopy and reported to be more active perpendicular to the grooves in contrast to more passive dynamics in parallel to the grooves[59]. These observations were not linked to having an influence on cell alignment or contact guidance because differences in breaking adhesive contacts by traction forces were not considered to explain the observations. While previous studies searched for differential molecular cell signaling mechanisms to explain contact guidance[60,61], our data indicate that contact guidance might be a filopodia traction force-mediated peeling process. The cell is guided only in the direction where the geometrical constraints allow the filopodial contacts to mature by forming a maximal number of adhesive bonds.

Finally, topography sensing is one of the most fundamental processes that cells exploit to interact with their environments, either during development, wound healing or metastatic invasion. Substrate-exploring functions of filopodia were suggested from experiments on 2D substrates, without noticing the steering role enabled by nanoNewton filopodia traction forces. Furthermore, we could find no previous study investigating the role of filopodia traction forces in real nanofibrillar 3D environments. While the community mostly searched for molecular recognition mechanisms to perhaps explain topography sensing, we show here that filopodia play a most significant role in topography sensing: the contact angle formed between a filopodium and any object determines whether the contact can be stabilized or will break. Since silicon nanowires and glass have the same tensile Young's modulus, but not the same bending elasticity, our data show that they solicit very different cellular responses. We thus predict that any synthetic or biological fiber that is free to swing around and align with filopodia will evoke a greatly different mechanosensation than bulk materials or interconnected fiber networks in which the fibers much better resist displacement. This is potentially significant in many physiological processes, since physically or enzymatically cleaved fibers (open-ended) are present in wound sites, whereas interconnected ECM fiber networks dominate in healthy tissues. Gaining insights into the mechanisms of topography sensing is also crucial to learn how to properly design biomaterials that have the ability to promote healing and tissue regeneration.

Methods

Substrate fabrication. Standard microscopy cover slips (22×22 mm, Menzel Gläser Nr.1) were sonicated in acetone (10 min), propanol (1 min) and rinsed in DI water (10 min). Cleaned and dried coverslips were spin coated with photoresist (maN 1410, microresist technology), exposed with UV light through a cromium-coated quartz

mask and developed in developer solution ma-D 533 (microresist technology). Patterned coverslips were dipped in 40 nm undiluted Au colloidal solution (BBInternational) for 2h and dried for 6h on a hotplate at 60°C. Photo resist was stripped with acetone, rinsed in propanol and DI water. Silicon nanowires were grown from surface immobilized Au nanoparticles in a LPCVD quartz tube furnace (PEO 603, ATV) using silane and hydrogen similar as described in[33]. Patterned and dry cover glasses were glued into a customized cover glass holder with silicon vacuum grease (Dow Corning, medium viscosity) generating a cell culture chamber for optical microscopy that can hold 1 ml liquid.

Fibronectin functionalization. In order to functionalize glass and oxidized nanowire surfaces with fibronectin, the patterned and nanowire-decorated surfaces were incubated for all experiments in 50 µg/ml human plasma fibronectin for 1 h and rinsed 6 times with PBS. Important note for proper FN coating of nanowire surfaces: The FN protein solution has to be added to PBS-submerged surfaces. E.g. immerse nanowires inside the microscopy chamber in 200 µl PBS and add 200 µl of 100 µg/ml FN solution. Fibronectin was isolated and purified from human blood plasma by affinity chromatography (Züricher Blutspendedienst Swiss Red Cross, Switzerland) following the established methods from Engvall and Ruoslahti (1977)[62] and Kubow et al. (2009)[43]. Rinsed cover glasses were kept in PBS until PBS was replaced by cell culture media, immediately before cell seeding.

Cell culture. All experiments were performed with primary normal human dermal foreskin fibroblasts (PromoCell) at low passages (5–8). Before seeding, cells were cultured in serum-free fibroblast growth media (PromoCell) in polystyrene cell culture dishes. At 60–70% confluency, cells were removed from cell culture dishes by treatment with 0.05% trypsin in PBS at 37°C. Trypsin inhibitor solution was added and cells were centrifuged at 1100 rpm for 2 minutes. The liquid was removed quickly and the cell pellet was re-immersed in 2 ml cell culture media at 37°C. Cells were added immediately to the microscopy chamber at 37°C in CO_2-controlled environment. The procedure from adding trypsin to cell seeding on patterned nanowire substrates did not last longer than 10 minutes.

Fluorescent labeling. Cell membranes were stained with DIO membrane dye (Molecular Probes) for live cell microscopy. Membrane dye was added to cell culture dishes two hours before trypsinization. The actin cytoskeleton was stained using phalloidin Alexa 546 (Invitrogen). Cells were washed with PBS, then permeabilized with 0.2% triton X 100 and 1% formalin for 2 minutes and fixed with 1% formalin for 10 minutes. Phalloidin was added in 400-fold dilution for 20 minutes. Cells were rinsed in PBS and imaged in the confocal microscope.

For live-cell imaging of the actin cytoskeleton, fibroblasts were transiently transfected with an actin-GFP construct and imaged under normal cell culture conditions at 37°C in a CO2-controlled environment. Transfected cells were kindly provided by Dr. Katharina Maniura (EMPA Sankt Gallen, Switzerland).

Optical microscopy. Optical microscopy (DIC/transmission and fluorescence) was performed with either an Olympus FluoView 1000 or Leica SP5 confocal laser scanning microscope, both equipped with 40× air and 63× oil immersion objectives that were used for this study.

Cell preparation for scanning electron microscopy (SEM). Cells were prepared for SEM imaging following a protocol adapted from Anne Meinel[47]. Cells were rinsed with PBS and chemically fixed in glutaraldehyde and sodium cacodylate solution (Karnovsky Fixate) for 2 hours. Liquid was exchanged by ethanol in a dillution series up to 100% ethanol (dried with silica beads). Ethanol was replaced by hexamethyldisilazan (HMDS) (MicroChemicals) in a dilution series up to 100% HMDS. HMDS was evaporated in a fume hood at room temperature. HMDS has a very volatile nature and low surface energies. It evaporates without causing drying artifacts on freely suspended filopodia.

Samples were imaged in SEM *without* metal sputter coating. Metal sputter coating reduces chemical contrast for backscattered electron detection and also induce additional mechanical artifacts to fragile biological samples. Metals deposited in thin layers in a thermal (plasma) process are deposited under strain, which can alter underlying fragile cellular structures, especially thin filopodia with diameters of only 100–120 nm. Normally electron damage to the samples surface is tried to be avoided by metal sputter coating, but for our purposes it was necessary to be able to actively cut filopodia inside the SEM chamber with a focused electron beam.

Scanning Electron microscopy. Scanning electron microscopy was performed utilizing a Zeiss Gemini Ultra 55 housed in the ETH FIRST laboratory (www.first.ethz.ch). This SEM system contains multiple electron detectors such as In-lens, secondary electrons and backscattered electrons. The Ultra 55 is additionally equipped with a 10 kV electron-beam booster inside the acceleration column which is of importance to get high spatial resolution scans with low acceleration voltages, which are required for biological specimen. The beam booster accelerates the electrons after extraction from the heated filament by a 10 kV larger acceleration voltage, as the user wants to apply. Before focusing and before the electron-beam hits the specimen, the electron beam is decelerated again by 10 kV. This allows focusing the electron-beam to very small diameters, while imaging is performed at low electron energies.

1. Gustafson, T. & Wolpert, L. Cellular mechanisms in the morphogenesis of the sea urchin larva. The formation of arms. *Exp Cell Res* **22**, 509–520 (1961).
2. Albrecht-Buehler, G. Filopodia of spreading 3T3 cells. Do they have a substrate-exploring function? *J Cell Biol* **69**, 275–286 (1976).
3. Nobes, C. D. & Hall, A. Rho, rac, and cdc42 GTPases regulate the assembly of multimolecular focal complexes associated with actin stress fibers, lamellipodia, and filopodia. *Cell* **81**, 53–62 (1995).
4. Davenport, R. W., Dou, P., Rehder, V. & Kater, S. B. A sensory role for neuronal growth cone filopodia. *Nature* **361**, 721–724 (1993).
5. Gomez, L., Budelli, R. & Pakdaman, K. Dynamical behavior of a pacemaker neuron model with fixed delay stimulation. *Physical review. E, Statistical, nonlinear, and soft matter physics* **64**, 061910 (2001).
6. Mallavarapu, A. & Mitchison, T. Regulated actin cytoskeleton assembly at filopodium tips controls their extension and retraction. *J. Cell Biol.* **146**, 1097–1106 (1999).
7. Bentley, D. & Toroian-Raymond, A. Disoriented pathfinding by pioneer neurone growth cones deprived of filopodia by cytochalasin treatment. *Nature* **323**, 712–715 (1986).
8. Chien, C. B., Rosenthal, D. E., Harris, W. A. & Holt, C. E. Navigational errors made by growth cones without filopodia in the embryonic Xenopus brain. *Neuron* **11**, 237–251 (1993).
9. Vasioukhin, V., Bauer, C., Yin, M. & Fuchs, E. Directed actin polymerization is the driving force for epithelial cell-cell adhesion. *Cell* **100**, 209–219 (2000).
10. Pula, G. *et al.* PKCdelta regulates collagen-induced platelet aggregation through inhibition of VASP-mediated filopodia formation. *Blood* **108**, 4035–4044 (2006).
11. Dalby, M. J., Gadegaard, N., Riehle, M. O., Wilkinson, C. D. & Curtis, A. S. Investigating filopodia sensing using arrays of defined nano-pits down to 35 nm diameter in size. *Int J Biochem Cell Biol* **36**, 2005–2015 (2004).
12. Curtis, A. & Wilkinson, C. New depths in cell behaviour: reactions of cells to nanotopography. *Biochem Soc Symp* **65**, 15–26 (1999).
13. Dalby, M., Riehle, M., Johnstone, H., Affrossman, S. & Curtis, A. In *Biomaterials* Vol. 23 2945–2954 (2002).
14. Jiang, H. & Grinnell, F. Cell-matrix entanglement and mechanical anchorage of fibroblasts in three-dimensional collagen matrices. *Mol Biol Cell* **16**, 5070–5076 (2005).
15. Sorkin, R. *et al.* Process entanglement as a neuronal anchorage mechanism to rough surfaces. *Nanotechnology* **20**, 015101 (015108pp) (2009).
16. Partridge, M. A. & Marcantonio, E. E. Initiation of attachment and generation of mature focal adhesions by integrin-containing filopodia in cell spreading. *Mol Biol Cell* **17**, 4237–4248 (2006).
17. Seymour, R. M. & Berry, M. Scanning and transmission electron microscope studies of interkinetic nuclear migration in the cerebral vesicles of the rat. *The Journal of comparative neurology* **160**, 105–125 (1975).
18. Bereiter-Hahn, J., Luck, M., Miebach, T., Stelzer, H. K. & Voth, M. Spreading of trypsinized cells: cytoskeletal dynamics and energy requirements. *J Cell Sci* **96** (Pt 1), 171–188 (1990).
19. Bohil, A. B., Robertson, B. W. & Cheney, R. E. Myosin-X is a molecular motor that functions in filopodia formation. *Proc. Natl Acad. Sci. USA* **103**, 12411–12416 (2006).
20. Dubin-Thaler, B. J., Giannone, G., Dobereiner, H. G. & Sheetz, M. P. Nanometer analysis of cell spreading on matrix-coated surfaces reveals two distinct cell states and STEPs. *Biophys J* **86**, 1794–1806 (2004).
21. Small, J. V., Stradal, T., Vignal, E. & Rottner, K. The lamellipodium: where motility begins. *Trends Cell Biol* **12**, 112–120 (2002).
22. Moore, S. W., Roca-Cusachs, P. & Sheetz, M. P. Stretchy proteins on stretchy substrates: the important elements of integrin-mediated rigidity sensing. *Dev Cell* **19**, 194–206 (2010).
23. Giannone, G. *et al.* Periodic lamellipodial contractions correlate with rearward actin waves. *Cell* **116**, 431–443 (2004).
24. Prager-Khoutorsky, M. *et al.* Fibroblast polarization is a matrix-rigidity-dependent process controlled by focal adhesion mechanosensing. *Nat Cell Biol* **13**, 1457–1465 (2011).
25. Cuvelier, D. *et al.* The Universal Dynamics of Cell Spreading. *Current Biology* **17**, 694–699 (2007).
26. Reinhart-King, C. A., Dembo, M. & Hammer, D. A. The dynamics and mechanics of endothelial cell spreading. *Biophys J* **89**, 676–689 (2005).
27. Schlunck, G. *et al.* Substrate rigidity modulates cell matrix interactions and protein expression in human trabecular meshwork cells. *Invest Ophthalmol Vis Sci* **49**, 262–269 (2008).
28. Mooney, D. J., Langer, R. & Ingber, D. E. Cytoskeletal filament assembly and the control of cell spreading and function by extracellular matrix. *J Cell Sci* **108 (Pt 6)**, 2311–2320 (1995).
29. Zaidel-Bar, R., Itzkovitz, S., Ma'ayan, A., Iyengar, R. & Geiger, B. Functional atlas of the integrin adhesome. *Nat Cell Biol* **9**, 858–867 (2007).
30. Mattila, P. K. & Lappalainen, P. Filopodia: molecular architecture and cellular functions. *Nat Rev Mol Cell Biol* **9**, 446–454 (2008).
31. Gupton, S. L. & Gertler, F. B. Filopodia: The Fingers That Do the Walking. *Sci. STKE* **2007**, re5– (2007).
32. Faix, J. & Rottner, K. The making of filopodia. *Curr. Opin. Cell Biol.* **18**, 18–25 (2006).
33. Albuschies, J. *et al.* High-density silicon nanowire growth from self-assembled Au nanoparticles. *Microelectronic Engineering* **83**, 1530–1533 (2006).

34. Kim, W., Ng, J. K., Kunitake, M. E., Conklin, B. R. & Yang, P. Interfacing silicon nanowires with mammalian cells. *J Am Chem Soc* **129**, 7228–7229 (2007).

35. Peer, E., Artzy-Schnirman, A., Gepstein, L. & Sivan, U. Hollow nanoneedle array and its utilization for repeated administration of biomolecules to the same cells. *ACS Nano* **6**, 4940–4946 (2012).

36. Berthing, T. *et al.* Intact mammalian cell function on semiconductor nanowire arrays: new perspectives for cell-based biosensing. *Small* **7**, 640–647 (2011).

37. Stan, G., Krylyuk, S., Davydov, A. V., Levin, I. & Cook, R. F. Ultimate bending strength of si nanowires. *Nano Lett* **12**, 2599–2604 (2012).

38. Hallstrom, W. *et al.* Fifteen-piconewton force detection from neural growth cones using nanowire arrays. *Nano Lett* **10**, 782–787 (2010).

39. Williams, B. R., Gelman, R. A., Poppke, D. C. & Piez, K. A. Collagen fibril formation. Optimal in vitro conditions and preliminary kinetic results. *J Biol Chem* **253**, 6578–6585 (1978).

40. Chen, L. B., Murray, A., Segal, R. A., Bushnell, A. & Walsh, M. L. Studies on intercellular LETS glycoprotein matrices. *Cell* **14**, 377–391 (1978).

41. Morita, M., Ohmi, T., Hasegawa, E., Kawakami, M. & Ohwada, M. Growth of Native Oxide on a Silicon Surface. *Journal of Applied Physics* **68**, 1272–1281 (1990).

42. Guillou, H. Lamellipodia nucleation by filopodia depends on integrin occupancy and downstream Rac1 signaling. *Exp. Cell Res.* **314**, 478–488 (2008).

43. Kubow, K. E. *et al.* Crosslinking of cell-derived 3D scaffolds up-regulates the stretching and unfolding of new extracellular matrix assembled by reseeded cells. *Integr Biol (Camb)* **1**, 635–648 (2009).

44. Cukierman, E., Pankov, R., Stevens, D. R. & Yamada, K. In *Science* Vol. **294**, 1708–1712 (2001).

45. Engler, A. J., Chan, M., Boettiger, D. & Schwarzbauer, J. E. A novel mode of cell detachment from fibrillar fibronectin matrix under shear. *J Cell Sci* **122**, 1647–1653 (2009).

46. Liu, X. *et al.* Guidance of neurite outgrowth on aligned electrospun polypyrrole/poly(styrene-beta-isobutylene-beta-styrene) fiber platforms. *Journal of biomedical materials research. Part A* **94**, 1004–1011 (2010).

47. Meinel, A. J. *et al.* Optimization strategies for electrospun silk fibroin tissue engineering scaffolds. *Biomaterials* **30**, 3058–3067 (2009).

48. San Paulo, A. *et al.* Mechanical elasticity of single and double clamped silicon nanobeams fabricated by the vapor-liquid-solid method. *Applied Physics Letters* **87**, 053111 (2005).

49. Hoffmann, S. *et al.* Measurement of the bending strength of vapor-liquid-solid grown silicon nanowires. *Nano Letters* **6**, 622–625 (2006).

50. Heidemann, S. R., Lamoureux, P. & Buxbaum, R. E. Growth cone behavior and production of traction force. *J Cell Biol* **111**, 1949–1957 (1990).

51. Bridgman, P. C., Dave, S., Asnes, C. F., Tullio, A. N. & Adelstein, R. S. Myosin IIB is required for growth cone motility. *J Neurosci* **21**, 6159–6169 (2001).

52. Théry, M. *et al.* The extracellular matrix guides the orientation of the cell division axis. *Nat Cell Biol* **7**, 947–953 (2005).

53. Fink, J. *et al.* External forces control mitotic spindle positioning. *Nat Cell Biol* **13**, 771–778 (2011).

54. Kufer, S. K., Puchner, E. M., Gumpp, H., Liedl, T. & Gaub, H. E. Single-molecule cut-and-paste surface assembly. *Science* **319**, 594–596 (2008).

55. Schmidt, C. & Vogel, V. Molecular shuttles powered by motor proteins: loading and unloading stations for nanocargo integrated into one device. *Lab on a Chip* **10**, 2195–2198 (2010).

56. Nordin, D., Donlon, L. & Frankel, D. Characterising single fibronectin-integrin complexes. *Soft Matter* **8**, 6151–6160 (2012).

57. Li, F., Redick, S. D., Erickson, H. P. & Moy, V. T. Force measurements of the alpha5beta1 integrin-fibronectin interaction. *Biophys J* **84**, 1252–1262 (2003).

58. Wojciak-Stothard, B., Curtis, A., Monaghan, W., MacDonald, K. & Wilkinson, C. Guidance and activation of murine macrophages by nanometric scale topography. *Exp Cell Res* **223**, 426–435 (1996).

59. Fujita, S., Ohshima, M. & Iwata, H. Time-lapse observation of cell alignment on nanogrooved patterns. *J R Soc Interface* **6 Suppl 3**, S269–277 (2009).

60. Calzado-Martán, A. *et al.* On the role of RhoA/ROCK signaling in contact guidance of bone-forming cells on anisotropic Ti6Al4V surfaces. *Acta Biomaterialia* **7**, 1890–1901 (2010).

61. Dalby, M. J., Hart, A. & Yarwood, S. J. The effect of the RACK1 signalling protein on the regulation of cell adhesion and cell contact guidance on nanometric grooves. *Biomaterials* **29**, 282–289 (2008).

62. Engvall, E. & Ruoslahti, E. Binding of soluble form of fibroblast surface protein, fibronectin, to collagen. *International journal of cancer. Journal international du cancer* **20**, 1–5 (1977).

63. Bershadsky, A., Balaban, N. & Geiger, B. Adhesion-dependent cell mechanosensitivity. *Annu. Rev. Cell. Dev. Biol.* **19**, 677–695 (2003).

Acknowledgements

Author contributions

J.A. and V.V. designed the research. J.A. performed it, prepared all figures and derived the mechanical model. J.A. and V.V. analyzed the data. J.A. and V.V. wrote the paper.

Additional information

Supplementary information accompanies this paper at http://www.nature.com/scientificreports

Competing financial interests: The authors declare no competing financial interests.

How to cite this article: Albuschies, J. & Vogel, V. The role of filopodia in the recognition of nanotopographies. *Sci. Rep.* **3**, 1658; DOI:10.1038/srep01658 (2013).